INVITED FEATURE PAPER

Rapid sol–gel synthesis of nanodiamond aerogel

Sandeep Manandhar,[b] Paden B. Roder,[b] Jennifer L. Hanson, and Matthew Lim
Department of Materials Science & Engineering, University of Washington, Seattle, Washington 98195, USA

Bennett E. Smith
Department of Chemistry, University of Washington, Seattle, Washington 98195, USA

Austin Mann
Department of Materials Science & Engineering, University of Washington, Seattle, Washington 98195, USA

Peter J. Pauzauskie[a]
Department of Materials Science & Engineering, University of Washington, Seattle, Washington 98195, USA; and Fundamental & Computational Sciences Directorate, Pacific Northwest National Laboratory Richland, Washington 99354, USA

(Received 9 July 2014; accepted 14 October 2014)

The rapid sol–gel synthesis of macroscopic quantities of nanodiamond aerogel (NDAG) is reported at standard temperature and pressure using acid-catalyzed covalent crosslinking of air-oxidized detonation nanodiamond (DND) nanocrystals. Acetonitrile acts as a polar, aprotic solvent both to form a colloidal dispersion of DND particles and to conduct acid-catalyzed polycondensation reactions between resorcinol and formaldehyde (RF) small molecule precursors. Several characterization techniques show that nanodiamond grains are connected via covalent bonding with RF molecules to form a porous, three-dimensional network. Solvent exchange into liquid carbon dioxide and subsequent supercritical drying of NDAGs are used to recover low-density (151 mg/cm^3), three-dimensional monolithic aerogels that exhibit surface areas in excess of 589 m^2/g. The large accessible pore volume from the rapidly synthesized, macroscopic NDAG materials suggests a range of potential applications in catalysis, sensing, energy storage, as well as inert excipients for small-molecule pharmaceuticals.

I. INTRODUCTION

The extreme physical and chemical properties[1] as well as low toxicity[2] of detonation nanodiamond (DND) materials have led to great interest, recently, in using these materials for both therapeutic and diagnostic applications in nanomedicine[3] and for electrochemical supercapacitors.[4] Currently, most of the nanodiamonds are manufactured through the detonation of explosives containing carbon followed by chemical purification of explosion-produced soot, which results in diamond grains with diameters in the range of single-digit-nanometers.[5] Nanodiamond materials are under investigation for biomedical imaging and drug-delivery applications based on their low toxicity and demonstrated biocompatibility.[2] Furthermore, negatively charged nitrogen-vacancy color centers can be used for bright, photostable biolabelling[6,7] applications based on extended red emission at ~700 nm and near-unit fluorescence quantum yield.[7–9]

Nanodiamond materials with high surface areas are of interest for numerous photocatalytic,[10,11] photonic,[12] astrophysical,[13–15] and drug-delivery applications.[3] Water-based nanodiamond gels have also been demonstrated to have a significant impact on the thermodynamic behavior of water confined within nanoscale pores.[16] High-pressure, high-temperature (HPHT) synthetic approaches have been reported recently to produce high surface area diamond aerogel materials in a laser-heated diamond anvil cell[17] as well as mesoporous diamond using a multianvil press.[18] These materials are of interest, since aerogels are lightweight, have high surface areas, and contain abundant open pores that can be readily loaded with drugs or other compounds to be used as an effective payload delivery vessel. However, HPHT processing is costly in terms of both capital equipment and processing time. Developing chemical approaches to high surface area diamond synthesis would greatly increase availability and reduce cost for a range of applied and fundamental scientific applications.[19] Here, we report a rapid, low-cost alternative for making diamond aerogels by forming covalent bonds between individual nanocrystalline grains using a sol–gel reaction between resorcinol and formaldehyde (RF) molecular precursors.

[a]Address all correspondence to this author.
e-mail: peterpz@uw.edu
[b]These authors contributed equally to this work.
This paper has been selected as an Invited Feature Paper.
DOI: 10.1557/jmr.2014.336

 © Materials Research Society 2014

https://doi.org/10.1557/jmr.2014.336 Published online by Cambridge University Press

II. EXPERIMENTAL

A. Oxidation

DND materials (ND90, Dynalene) were oxidized in ambient air within a tube furnace (Lindberg Blue) at 450 °C for 8 h to remove amorphous carbon soot and to generate chemically reactive surface oxygen functional groups (carboxylic acids, anhydrides, etc.).[20,21] It has been experimentally shown that the oxidation process serves to reduce the size of the nanodiamonds, removes graphitic material, and increases the intensity of the nitrogen-vacancy centers within the nanodiamonds.[22] The final oxidized nanodiamond (OxDND) was used during synthesis and subsequent characterization of the nanodiamond aerogels (NDAGs).

B. Neutron activation analysis (NAA)

NAA was used to quantify the trace impurity content in the precursor and oxidized nanodiamonds. NAA technique is preferred for trace element quantification due to its high sensitivity and accurate, consistent, fast results with minimal sample preparation.[23] The samples are bombarded with neutrons to form radioactive nuclides. These radioactive nuclides decay, emitting gamma rays that can be quantitatively monitored. Decay schemes can be single events or sequential multistep progressions,[24] as is the case for Ce-133. The NAA data presented in this study were obtained using a TRIGA Mark II nuclear reactor. The samples (10 mg each) were enclosed in polyethylene capsules and were irradiated for 30 min. The study was performed at a thermal operating power of 100 kW, 4×10^{12} neutrons/cm^2 s thermal flux, and 4.8×10^{12} neutrons/cm^2 s fast and epithermal flux. Each sample was counted while positioned near the surface of a 25 cm^2, trapezohedral, germanium, lithium-drifted semiconductor detector (Nuclear Diodes), which is constantly cooled by liquid nitrogen (77 K). The dead time between the end of irradiation and the start of collection was 5 min. Ratiometric analyses were performed comparing experimental activities (μCi/unit) to calculated activities per given element and reactor efficiency to determine the concentrations of metallic impurities.

C. Synthesis

NDAGs were prepared using OxDND materials based on a modified time-efficient, acid-catalyzed method[25] for preparing resorcinol–formaldehyde aerogels. Briefly, 1.67 mL of high purity acetonitrile (AN) (OmniSolv) was sonicated with 17.5 mg of DNDs for 15 min in polypropylene tubes. Following dispersion of OxDND within the AN solvent, 37.6 mg of resorcinol (R, Sigma-Aldrich) and 49.4 μL of formaldehyde (F, Sigma-Aldrich, 37% w/w aqueous solution with methanol as a stabilizer) were added to the mixture and sonicated for 20 min until all the resorcinol was dissolved (1:2 molar ratio of R:F). Lastly, 4 μL of HCl (C, Sigma-Aldrich, 37% ACS reagent) was added as a catalyst and the mixture was further sonicated for 30 min (8:1 molar ratio R:C).

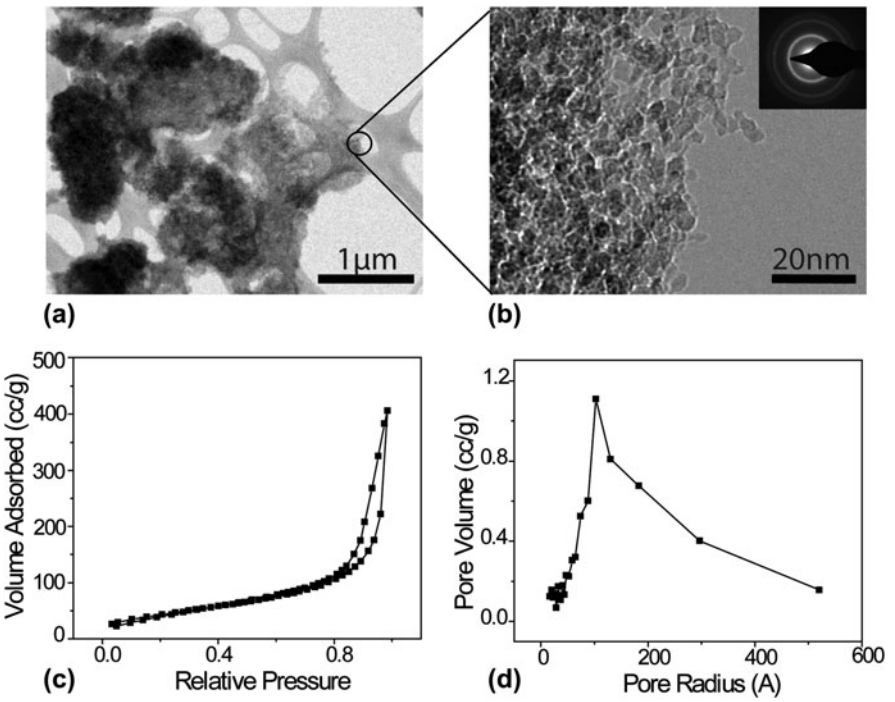


FIG. 1. (a) BF-TEM of OxDND clusters. (b) BF-TEM images of OxDND at a higher magnification, showing that clusters are formed from the aggregation of smaller nanodiamond crystal grains. (c) Nitrogen adsorption isotherm. (d) Pore size distribution of OxDND.

https://doi.org/10.1557/jmr.2014.336 Published online by Cambridge University Press

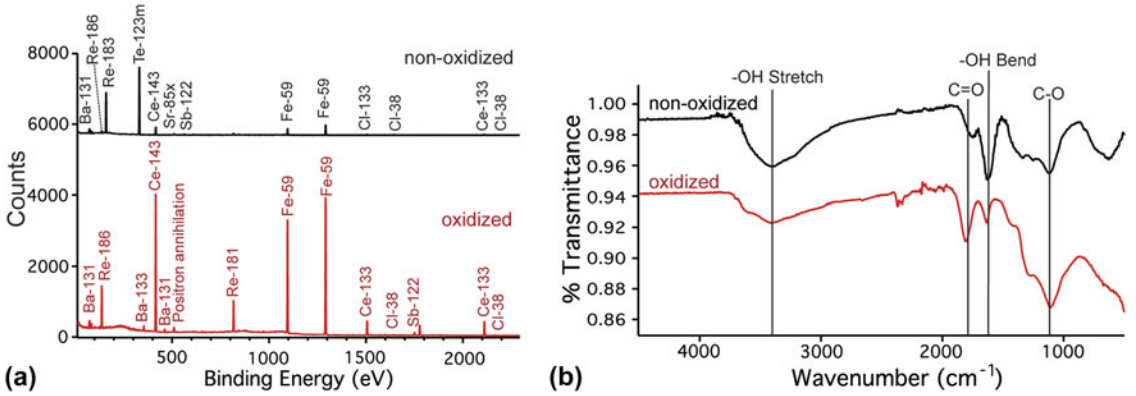


FIG. 2. (a) NAA of ND90 (black) and OxDND (red) precursor. (b) FTIR of ND90 (black) and OxDND (red) precursor.

TABLE I. List of elements identified by NAA.

Nuclide	Precursor concentration (ND90)	Oxidized concentration (OxDND)
Cl-38	159 ppt	163 ppt
Fe-59	29 ppm	494 ppm
Sr-85x	655 ppb	6 ppt
Ru-103	197 ppt	No trace
Te-123m	443 ppb	No trace
Re-186	37 ppt	492 ppt
Ba-133	5 ppb	95 ppb
Ba-131	4 ppm	6 ppm

The R:OxDND mass ratio used for the sol–gel reaction was 2:1. The mixture (sol) gelled within 30 min at room temperature during sonication. The resulting NDAG molar ratio of R:AN was 1:94. The gels were then washed with anhydrous ethanol (4× over 48 h) and supercritically dried in CO_2 (E3100 critical point dryer, Quorum Technologies, Laughton, East Sussex, UK). Supercritical point drying (SCPD) was used to dry the wet gel to preserve the porosity of the solid matrix.

D. Surface area and pore volume

Surface area and pore volume measurements were performed by the Brunauer–Emmett–Teller (BET) and Barrett–Joyner–Halenda (BJH) methods, respectively, using a Nova 2200e analyzer (Quantachrome) with nitrogen gas as the adsorbate. The OxDND was degassed for 17 h at 125 °C prior to performing the BET measurement while the NDAG was loaded in the analyzer immediately following SCPD. High temperature degassing was avoided given discoloration of the aerogel that was observed at 200 °C.

E. Electron microscopy

The NDAG material was analyzed by using a FEI Sirion scanning electron microscope (SEM). Samples were prepared for SEM characterization by coating the material with a 10 nm layer of sputtered gold. The samples were also analyzed using transmission electron microscopy (TEM, FEI Tecnai G2 F20, Hillsboro, OR, 200 kV accelerating voltage) to verify the presence of nanodiamonds within the RF matrix. High-resolution bright field (HR-BF) imaging, select area electron diffraction (SAED), and high angle annular dark-field (HAADF) scanning transmission imaging were performed to characterize the NDAG microstructure.

F. Fourier transform infrared spectroscopy (FTIR)

Attenuated total reflectance FTIR (ATR-FTIR) spectroscopy was performed using a Bruker VERTEX 70 Fourier transform infrared spectrometer (Billerica, MA) with an integrated Platinum-ATR-accessory (Unit A225/Q1). The resulting data were used to identify the functional groups, impurities, and adsorbed molecules on the surface of the precursor materials and synthesized aerogels.

G. X-ray diffraction (XRD)

XRD was performed using a Bruker D8 Discover x-ray diffractometer equipped with a General Area Detector Diffraction Systems (GADDS) XRD system using a Cu K_α source. Powder samples were aligned in the system using the laser guidance system provided in the instrument.

III. RESULTS AND DISCUSSION

A. Precursor characterization

TEM images of the precursor OxDND [Figs. 1(a) and 1(b)] show that the nanodiamonds are aggregated into clusters of roughly 1 μm diameter, being made up of smaller crystalline grains of approximately 5 nm in diameter. The OxDND is polycrystalline, as verified by the SAED pattern shown in the inset of Fig. 1(b). In addition, the BET surface area of the OxDND, as calculated from the nitrogen adsorption/desorption isotherm in Fig. 1(c), is 161 m^2/g,

https://doi.org/10.1557/jmr.2014.336 Published online by Cambridge University Press

which supports the fact that the nanodiamond clusters have a high surface area. The pore volume distribution in Fig. 1(d) shows that the OxDND has an average pore volume of 0.613 cm³/g.

The quality, physical/chemical properties, and potential use in specific applications of nanodiamonds depend critically on the purity of the material. The purity of the nanodiamond is determined by oxidative isolation of the diamond fraction from the synthetic detonation soot (predominately graphitic carbon) and by the remaining noncarbon impurities originating from the source of explosive materials, walls of the detonation chamber, and detonator. The variation of these noncarbon impurities is extensive and includes both metal (Fe, Ti, Al, Cr, Si, etc.) and nonmetal (S, P, B, etc.) elements by up to 8 wt%.[26]

NAA was used to characterize these impurities for powder precursors used in this experiment. The NAA data in Fig. 2(a) show that several metallic impurities (rhenium, ruthenium, cerium, and iron) are present in the analyzed samples. The elements chlorine, barium, tellurium, strontium, and antimony comprise the nonmetallic impurities. In general, there is significant variation in the impurities of the precursor nanodiamonds. Iron and cerium were present in all the samples and generally increase in concentration during the oxidation process of nanodiamonds. In as-received DND material, the concentration of iron is observed to increase from 29 ppm to

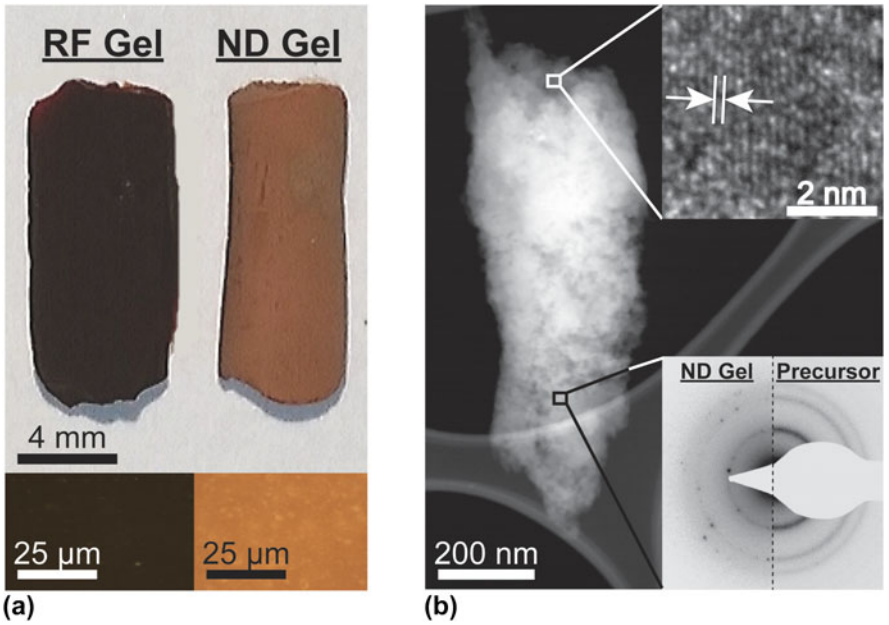


FIG. 3. (a) Digital photograph showing side-by-side color comparison of RF and NDAGs following supercritical drying. Corresponding dark field optical microscopy images are shown below for each material at 100x magnification. (b) HAADF TEM of the nanodiamond aerogel. Insets: HR-TEM showing lattice of a nanodiamond embedded within the aerogel (top-right), and a comparison of the SAED of the nanodiamonds in the aerogel compared to the nanodiamond precursor (bottom-right).

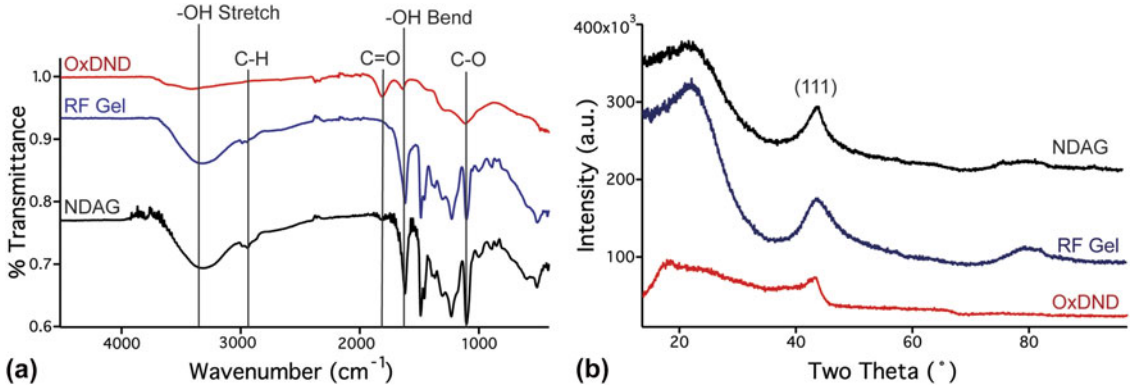


FIG. 4. (a) FTIR spectra of OxDND (red), pure RF aerogel (blue), and NDAG (black). (b) XRD spectra of OxDND (red), RF aerogel (blue), and NDAG (black).

https://doi.org/10.1557/jmr.2014.336 Published online by Cambridge University Press

nearly 500 ppm following air oxidation. The mass of carbon in a given sample is reduced during the oxidation process following the formation of gas-phase CO_2 and CO molecules. In contrast to carbon, iron does not form volatile oxidation by-products at this oxidation temperature (450 °C), resulting in an increase in the residual concentration of iron. Furthermore, the results indicate that the oxidation process tends to remove the trace elements ruthenium and tellurium. The list of elements identified by NAA in precursor nanodiamond (ND90) and OxDND is given in Table I.

FTIR spectra shown in Fig. 2(b) indicate that all of the spectra show the surface hydroxyl (O–H) vibration bands (stretch regions from 3650 to 2920 cm^{-1} and bend regions from 1510 to 1700 cm^{-1})[20,27,28] and C=O bonds of carboxylic acid (region from 1700 to 1880 cm^{-1}).[28,29]

TABLE II. Wave numbers of absorption peaks in FTIR spectra.

	ND90	OxDND	RF gel	NDAG
–OH stretch	3400	3406	3321	3300, 3790
–OH bend	1630	1628	1610	1608
C–H stretch	...	...	2975	2930, 2970
C=O	1755	1800	...	1800
C–O	1115, 1250, 1335	1100, 1273	1093, 1217, 1294, 1360	1092, 1219, 1294, 1367, 1379
–C=C–H	627	...	987	987
C–H out-of-plane ('oop')	...	...	879	839, 877
$–CH_2–$	...	...	1445, 1475	1444, 1475

Also, the peak near 1100 cm^{-1} is related to C–O stretching vibration present in the DND and OxDND.[30] The small peak on the OxDND spectrum near 2324–2360 cm^{-1} is due to adsorbed molecules of CO_2.[29]

B. Diamond aerogel characterization

There is a dramatic lightening in color of the recovered NDAG material in comparison with pure RF aerogel, as shown in Fig. 3(a). The final color of the NDAG is pinkish-white in contrast to the deep-red color of the RF aerogel at an identical R:AN ratio. Despite the contrast in color, both RF and NDAG were similar in shape and mechanical stability and easily held under standard handling and analytic procedures. TEM SAED [Fig. 3(b), inset] confirms the presence of OxDND in the aerogel matrix, showing a polycrystalline ring pattern. HAADF TEM [Fig. 3(b)] shows that the NDAG samples exhibit a highly porous microstructure that is maintained following SCPD.

Figures 2(b) and 4(a) show FTIR spectra taken in air of the ND90 precursor, OxDND, the RF aerogel control, and NDAG samples. Due to the oxidative nature of the detonation, as well as the air oxidation of the precursor nanodiamonds, the surface of the OxDND contains various oxygen-containing groups. All samples show C–O–C stretching bands from ethers, acid anhydrides, lactones, and epoxy groups in the region 1100–1370 cm^{-1}.[31] Adsorbed water gives strong absorption bands in the 3500–3300 and 1620–1630 cm^{-1} (bending mode) regions. Carbonyl C=O peaks (1700–1865 cm^{-1} for

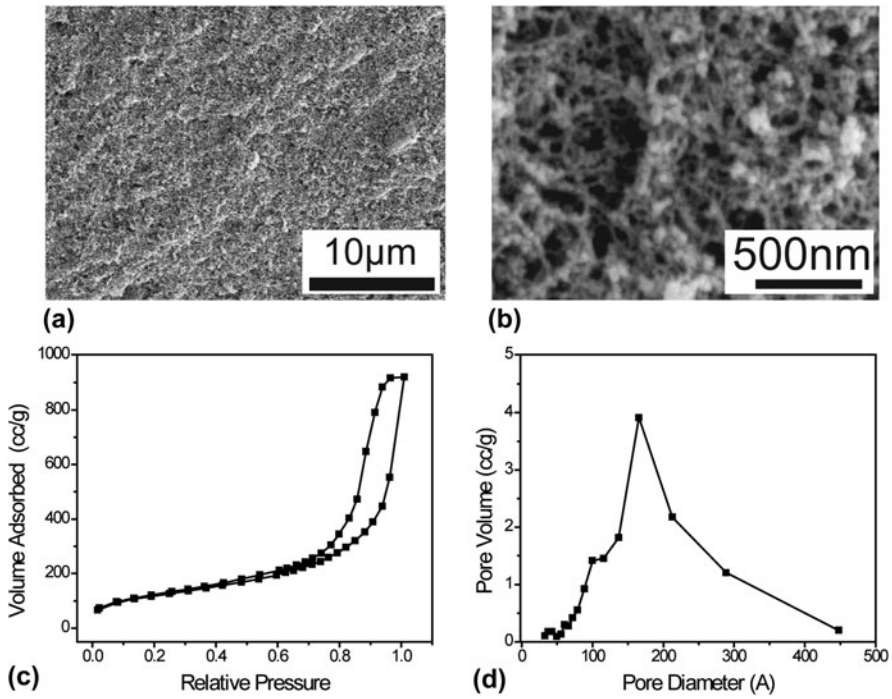


FIG. 5. (a) SEM image of unpyrolyzed NDAG. (b) High-magnification SEM image of NDAG. (c) Nitrogen adsorption/desorption isotherm, and (d) BJH pore size distribution of NDAG.

https://doi.org/10.1557/jmr.2014.336 Published online by Cambridge University Press

carbonyls in ketones, carboxylic acids, acid anhydrides, esters, and lactones) are not observed in the pure RF gel but appear in the NDAG due to the addition of nanodiamonds, which contain these bonds. Also, neither of the precursor nanodiamonds show the presence of C–H or CH_2 stretching, as opposed to the RF aerogel and NDAG, since they are not bonded with any resorcinol/formaldehyde condensation polymers. The wave numbers of the absorption peaks corresponding to each vibrational mode identified by the FTIR are shown in Table II.

Analysis of the XRD spectra indicates the presence of amorphous hydrocarbons within both RF and NDAG samples following sol–gel cross-linking reactions. The peak at around $2\theta = 43°$ is the characteristic (111) diffraction peak of diamond.[32] Both aerogels exhibit an additional broader, weaker peak at $2\theta = 75°$, indicating that they are partially graphitic.[33–35]

The microstructure of recovered NDAG materials was observed further using SEM. The surface of the NDAG appears to be highly porous as shown in Figs. 5(a) and 5(b). Figures 5(c) and 5(d) show the nitrogen adsorption/desorption isotherm and pore size distribution, respectively, of the NDAG with R:AN molar ratio of 1:94 and R:OxDND weight ratio of 2:1. The micropore surface area for this gel is 589 m^2/g. Bulk density was approximated by dividing the measured mass of a typical sample over its macroscopic volume and was found to be ~151 mg/cm^3.

IV. CONCLUSION

In conclusion, a fast sol–gel process is reported for preparing macroscopic quantities of NDAG materials with high surface areas based on acid-catalyzed condensation reactions in a polar, aprotic solvent (acetonitrile). Metallic impurities within detonation nanodiamond precursor materials were analyzed using NAA, and air oxidation was observed to increase the amount of iron by approximately one order of magnitude. Transmission electron microscopy was used to show that the NDAG material contains nanodiamonds dispersed throughout the resorcinol–formaldehyde matrix. Future efforts will focus on optimizing the microstructure of NDAG for loading with small-molecule pharmaceuticals, as well as tuning the density and mechanical properties for potential applications in future STARDUST missions.[19]

ACKNOWLEDGMENTS

The authors gratefully acknowledge the financial support from the University of Washington startup funding and the ACS Petroleum Research Fund. The authors also thank G. Cao for access to SCPD facilities. This work was performed under the auspices of the U.S. Department of Energy and the Fundamental & Computational Sciences Division of the Pacific Northwest National Laboratory. The PNNL is operated by Battelle under contract #DE-AC05-76RL01830. PBR acknowledges the support from the National Science Foundation Graduate Research Fellowship under Grant No. DGE-1256082.

REFERENCES

1. V.N. Mochalin, O. Shenderova, D. Ho, and Y. Gogotsi: The properties and applications of nanodiamonds. *Nat. Nanotechnol.* **7**(1), 11 (2012).
2. C-C. Fu, H-Y. Lee, K. Chen, T-S. Lim, H-Y. Wu, P-K. Lin, P-K. Wei, P-H. Tsao, H-C. Chang, and W. Fann: Characterization and application of single fluorescent nanodiamonds as cellular biomarkers. *Proc. Natl. Acad. Sci. U.S.A.* **104**(3), 727 (2007).
3. H-J. Kim, K. Zhang, L. Moore, and D. Ho: Diamond nanogel-embedded contact lenses mediate lysozyme-dependent therapeutic release. *ACS Nano* **8**, 2998–3005 (2014).
4. Q. Wang, N. Plylahan, M.V. Shelke, R.R. Devarapalli, M.S. Li, P. Subramanian, T. Djenizian, R. Boukherroub, and S. Szunerits: Nanodiamond particles/reduced graphene oxide composites as efficient supercapacitor electrodes. *Carbon* **68**, 175 (2014).
5. O. Shenderova, A.M. Panich, S. Moseenkov, S.C. Hens, V. Kuznetsov, and H.M. Vieth: Hydroxylated detonation nanodiamond: FTIR, XPS, and NMR studies. *J. Phys. Chem. C* **115** (39), 19005 (2011).
6. N. Mohan, Y-K. Tzeng, L. Yang, Y-Y. Chen, Y.Y. Hui, C-Y. Fang, and H-C. Chang: Sub-20-nm fluorescent nanodiamonds as photostable biolabels and fluorescence resonance energy transfer donors. *Adv. Mater.* **22**(7), 843 (2010).
7. S.J. Yu, M.W. Kang, H.C. Chang, K.M. Chen, and Y.C. Yu: Bright fluorescent nanodiamonds: No photobleaching and low cytotoxicity. *J. Am. Chem. Soc.* **127**(50), 17604 (2005).
8. Y.R. Chang, H.Y. Lee, K. Chen, C.C. Chang, D.S. Tsai, C.C. Fu, T.S. Lim, Y.K. Tzeng, C.Y. Fang, C.C. Han, H.C. Chang, and W. Fann: Mass production and dynamic imaging of fluorescent nanodiamonds. *Nat. Nanotechnol.* **3**(5), 284 (2008).
9. F. Neugart, A. Zappe, F. Jelezko, C. Tietz, J.P. Boudou, A. Krueger, and J. Wrachtrup: Dynamics of diamond nanoparticles in solution and cells. *Nano Lett.* **7**(12), 3588 (2007).
10. D. Zhu, L.H. Zhang, R.E. Ruther, and R.J. Hamers: Photo-illuminated diamond as a solid-state source of solvated electrons in water for nitrogen reduction. *Nat. Mater.* **12**(9), 836 (2013).
11. K.D. Kim, N.K. Dey, H.O. Seo, Y.D. Kim, D.C. Lim, and M. Lee: Photocatalytic decomposition of toluene by nanodiamond-supported TiO2 prepared using atomic layer deposition. *Appl. Catal., A* **408**(1–2), 148 (2011).
12. I.I. Vlasov, A.A. Shiryaev, T. Rendler, S. Steinert, S-Y. Lee, D. Antonov, M. Voros, F. Jelezko, A.V. Fisenko, L.F. Semjonova, J. Biskupek, U. Kaiser, O.I. Lebedev, I. Sildos, P.R. Hemmer, V.I. Konov, A. Gali, and J. Wrachtrup: Molecular-sized fluorescent nanodiamonds. *Nat. Nanotechnol.* **9**(1), 54 (2014).
13. H.C. Chang, K.W. Chen, and S. Kwok: Nanodiamond as a possible carrier of extended red emission. *Astrophys. J.* **639**(2), L63 (2006).
14. G.K. Ustinova: Production of anomalous Xe in nanodiamond in chondrites during the last supernova explosion predating the origin of the solar system. *Geochem. Int.* **49**(6), 555 (2011).
15. A.P. Jones: The mineralogy of cosmic dust: Astromineralogy. *Eur. J. Mineral.* **19**(6), 771 (2007).
16. M.V. Korobov, N.V. Avramenko, A.G. Bogachev, N.N. Rozhkova, and E. Ōsawa: Nanophase of water in nano-diamond gel. *J. Phys. Chem. C* **111**(20), 7330 (2007).

https://doi.org/10.1557/jmr.2014.336 Published online by Cambridge University Press

17. P.J. Pauzauskie, J.C. Crowhurst, M.A. Worsley, T.A. Laurence, A.L.D. Kilcoyne, Y. Wang, T.M. Willey, K.S. Visbeck, S.C. Fakra, W.J. Evans, J.M. Zaug, and J.H. Satcher, Jr.: Synthesis and characterization of a nanocrystalline diamond aerogel. *Proc. Natl. Acad. Sci. U.S.A.* **108**(21), 8550 (2011).
18. M. Mandal and K. Landskron: Synthetic chemistry with periodic mesostructures at high pressure. *Acc. Chem. Res.* **46**(11), 2536 (2013).
19. D. Brownlee, P. Tsou, J. Aleon, C.M.O. Alexander, T. Araki, S. Bajt, G.A. Baratta, R. Bastien, P. Bland, P. Bleuet, J. Borg, J.P. Bradley, A. Brearley, F. Brenker, S. Brennan, J.C. Bridges, N.D. Browning, J.R. Brucato, E. Bullock, M.J. Burchell, H. Busemann, A. Butterworth, M. Chaussidon, A. Cheuvront, M.F. Chi, M.J. Cintala, B.C. Clark, S.J. Clemett, G. Cody, L. Colangeli, G. Cooper, P. Cordier, C. Daghlian, Z.R. Dai, L. D'Hendecourt, Z. Djouadi, G. Dominguez, T. Duxbury, J.P. Dworkin, D.S. Ebel, T.E. Economou, S. Fakra, S.A.J. Fairey, S. Fallon, G. Ferrini, T. Ferroir, H. Fleckenstein, C. Floss, G. Flynn, I.A. Franchi, M. Fries, Z. Gainsforth, J.P. Gallien, M. Genge, M.K. Gilles, P. Gillet, J. Gilmour, D.P. Glavin, M. Gounelle, M.M. Grady, G.A. Graham, P.G. Grant, S.F. Green, F. Grossemy, L. Grossman, J.N. Grossman, Y. Guan, K. Hagiya, R. Harvey, P. Heck, G.F. Herzog, P. Hoppe, F. Horz, J. Huth, I.D. Hutcheon, K. Ignatyev, H. Ishii, M. Ito, D. Jacob, C. Jacobsen, S. Jacobsen, S. Jones, D. Joswiak, A. Jurewicz, A.T. Kearsley, L.P. Keller, H. Khodja, A.L.D. Kilcoyne, J. Kissel, A. Krot, F. Langenhorst, A. Lanzirotti, L. Le, L.A. Leshin, J. Leitner, L. Lemelle, H. Leroux, M.C. Liu, K. Luening, I. Lyon, G. MacPherson, M.A. Marcus, K. Marhas, B. Marty, G. Matrajt, K. McKeegan, A. Meibom, V. Mennella, K. Messenger, S. Messenger, T. Mikouchi, S. Mostefaoui, T. Nakamura, T. Nakano, M. Newville, L.R. Nittler, I. Ohnishi, K. Ohsumi, K. Okudaira, D.A. Papanastassiou, R. Palma, M.E. Palumbo, R.O. Pepin, D. Perkins, M. Perronnet, P. Pianetta, W. Rao, F.J.M. Rietmeijer, F. Robert, D. Rost, A. Rotundi, R. Ryan, S.A. Sandford, C.S. Schwandt, T.H. See, D. Schlutter, J. Sheffield-Parker, A. Simionovici, S. Simon, I. Sitnitsky, C.J. Snead, M.K. Spencer, F.J. Stadermann, A. Steele, T. Stephan, R. Stroud, J. Susini, S.R. Sutton, Y. Suzuki, M. Taheri, S. Taylor, N. Teslich, K. Tomeoka, N. Tomioka, A. Toppani, J.M. Trigo-Rodriguez, D. Troadec, A. Tsuchiyama, A.J. Tuzzolino, T. Tyliszczak, K. Uesugi, M. Velbel, J. Vellenga, E. Vicenzi, L. Vincze, J. Warren, I. Weber, M. Weisberg, A.J. Westphal, S. Wirick, D. Wooden, B. Wopenka, P. Wozniakiewicz, I. Wright, H. Yabuta, H. Yano, E.D. Young, R.N. Zare, T. Zega, K. Ziegler, L. Zimmerman, E. Zinner, and M. Zolensky: Comet 81P/Wild 2 under a microscope. *Science* **314**(5806), 1711 (2006).
20. S. Osswald, G. Yushin, V. Mochalin, S.O. Kucheyev, and Y. Gogotsi: Control of sp2/sp3 carbon ratio and surface chemistry of nanodiamond powders by selective oxidation in air. *J. Am. Chem. Soc.* **128**(35), 11635 (2006).
21. A. Kruger, Y. Liang, G. Jarre, and J. Stegk: Surface functionalisation of detonation diamond suitable for biological applications. *J. Mater. Chem.* **16**(24), 2322 (2006).
22. T. Gaebel, C. Bradac, J. Chen, J.M. Say, L. Brown, P. Hemmer, and J.R. Rabeau: Size-reduction of nanodiamonds via air oxidation. *Diamond Relat. Mater.* **21**(0), 28 (2012).
23. S. Yusuf, M. Krahenbuhl, B. Haskins, and M. Hartman: Improving neutron activation analysis accuracy for the measurement of gold in the characterization of heterogeneous catalysts using a TRIGA reactor. *J. Radioanal. Nucl. Chem.* **296**(1), 23 (2013).
24. D. Soete, R. Gijbels, and J. Hoste: *Neutron Activation Analysis* (Wiley-Interscience, London and New York, 1972).
25. S. Mulik, C. Sotiriou-Leventis, and N. Leventis: Time-efficient acid-catalyzed synthesis of resorcinol-formaldehyde aerogels. *Chem. Mater.* **19**(25), 6138 (2007).
26. D.P. Mitev, A.T. Townsend, B. Paull, and P.N. Nesterenko: Direct sector field ICP-MS determination of metal impurities in detonation nanodiamond. *Carbon* **60**(0), 326 (2013).
27. S. Ji, T. Jiang, K. Xu, and S. Li: FTIR study of the adsorption of water on ultradispersed diamond powder surface. *Appl. Surf. Sci.* **133**(4), 231 (1998).
28. T. Jiang and K. Xu: FTIR study of ultradispersed diamond powder synthesized by explosive detonation. *Carbon* **33**(12), 1663 (1995).
29. V.L. Kuznetsov, M.N. Aleksandrov, I.V. Zagoruiko, A.L. Chuvilin, E.M. Moroz, V.N. Kolomiichuk, V.A. Likholobov, P.M. Brylyakov, and G.V. Sakovitch: Study of ultradispersed diamond powders obtained using explosion energy. *Carbon* **29**(4–5), 665 (1991).
30. W.S. Yeap, Y.Y. Tan, and K.P. Loh: Using detonation nanodiamond for the specific capture of glycoproteins. *Anal. Chem.* **80**(12), 4659 (2008).
31. J.B. Lambert, H.F. Shurvell, and R.G. Cooks: *Introduction to Organic Spectroscopy*, 1st ed. (Macmillan, New York, 1987).
32. T. Sharda, M.M. Rahaman, Y. Nukaya, T. Soga, T. Jimbo, and M. Umeno: Structural and optical properties of diamond and nanodiamond films grown by microwave plasma chemical vapor deposition. *Diamond Relat. Mater.* **10**(3–7), 561 (2001).
33. C. Lin and J.A. Ritter: Effect of synthesis pH on the structure of carbon xerogels. *Carbon* **35**(9), 1271 (1997).
34. L.C. Cotet, V. Danciu, V. Cosoveanu, I.C. Popescu, R. Anna, and E. Molins: Synthesis of meso- and macroporous carbon aerogels. *Rev. Roum. Chim.* **52**(11), 1077 (2007).
35. M.S. Song, S. Nahm, and Y.J. Oh: Preparation and electrochemical properties of carbon cryogel for supercapacitor. *J. Korean Ceram. Soc.* **45**(11), 662 (2008).

https://doi.org/10.1557/jmr.2014.336 Published online by Cambridge University Press